An airborne expendable bathythermograph survey of the South China Sea, May 1995

Peter C. Chu and Chenwu Fan

Department of Oceanography, Naval Postgraduate School, Monterey, California

Carlos J. Lozano

Department of Earth and Planetary Sciences, Harvard University, Cambridge, Massachusetts

Jeffrey L. Kerling

Naval Oceanographic Office, Stennis Space Center, Mississippi

Abstract. An extensive airborne expendable bathythermograph survey of the South China Sea (SCS) conducted in May 1995 and historical data are used to analyze and infer the upper layer (300 m) synoptic structure and general circulation. The primary thermal feature observed was a central SCS warm pool surrounded by several cool pools. The size of the warm pool decreased with depth from approximately 200,000 km^2 at 50 m depth to about 70,000 km^2 at 300 m depth. The maximum temperature of the warm pool was 30°C, appearing near the surface. At the depth of 50 m, the temperature of the central SCS warm pool was 29°C, and the temperature of the five surrounding cool pools ranged from 26°C to 22°C. A three-dimensional estimate of the absolute velocity field was obtained from the observed temperature field and a climatological salinity field using the β spiral method. Striking circulation features were the existence of dual anticyclonic eddies in the central SCS warm pool and the existence of cyclonic eddies associated with the cool pools. In the upper layer the tangential velocity of the dual central SCS anticyclonic warm-core eddies is around 30-40 cm/s and that of the five cyclonic cool-core eddies varies from 10 cm/s to 40 cm/s. The tangential velocity of all the eddies decreased with depth. At 300 m depth, it became less than 5 cm/s for all the eddies.

1. Introduction

The South China Sea (SCS) has a bottom topography (Figure 1) that makes it a unique semi-enclosed ocean basin that is temporally forced by a pronounced monsoon wind. Extended continental shelves (less than 100 m deep) exist along the north boundary and across the southwest portion of the basin, while steep slopes with almost no shelf are found along the eastern boundary. The deepest water is confined to an oblate bowl oriented SW-NE, centered around 13°N. The maximum depth is around 4500 m.

The SCS's physical oceanography has been investigated for several decades. Studies show that eddies in SCS are predominantly cyclonic in winter and anticyclonic in summer, with sizes ranging from small to mesoscale, and both cold and warm eddies exist in SCS [Huang et al., 1994]. A survey by Wyrtki [1961] revealed complex temporal and spatial features of the surface

currents in both the SCS and the surrounding waters. By April, the northeast monsoon has decayed, and the main SCS current consists of two large cyclonic eddies in the western SCS, one in the north and the other in the south (Figure 2a). With the beginning of the southwest monsoon in May and June, a wind drift current is formed. Off the coast of Vietnam, westward intensification of this current is clearly visible. The wide, uniform drift in the northern SCS shows a deflection of the current to the right of the wind. A large part of the water passes south of Taiwan and into the root of the Kuroshio. The southern SCS is occupied by an anticyclonic eddy (Figure 2b).

Seasonal occurrence of SCS eddies have been reported by several authors. Dale [1956] and Uda and Nakao [1972] reported a cold eddy off the central Vietnam coast in summer. Nitani [1970] found a cold eddy located northwest of Luzon in summer. Reports from the South China Sea Institute of Oceanology (SCSIO) [1985] indicate that a warm-core eddy appears in summer and winter in the central SCS, but in summer, it is closer to Vietnam at the surface. Recently, a cold-core eddy was detected in the central SCS during De-
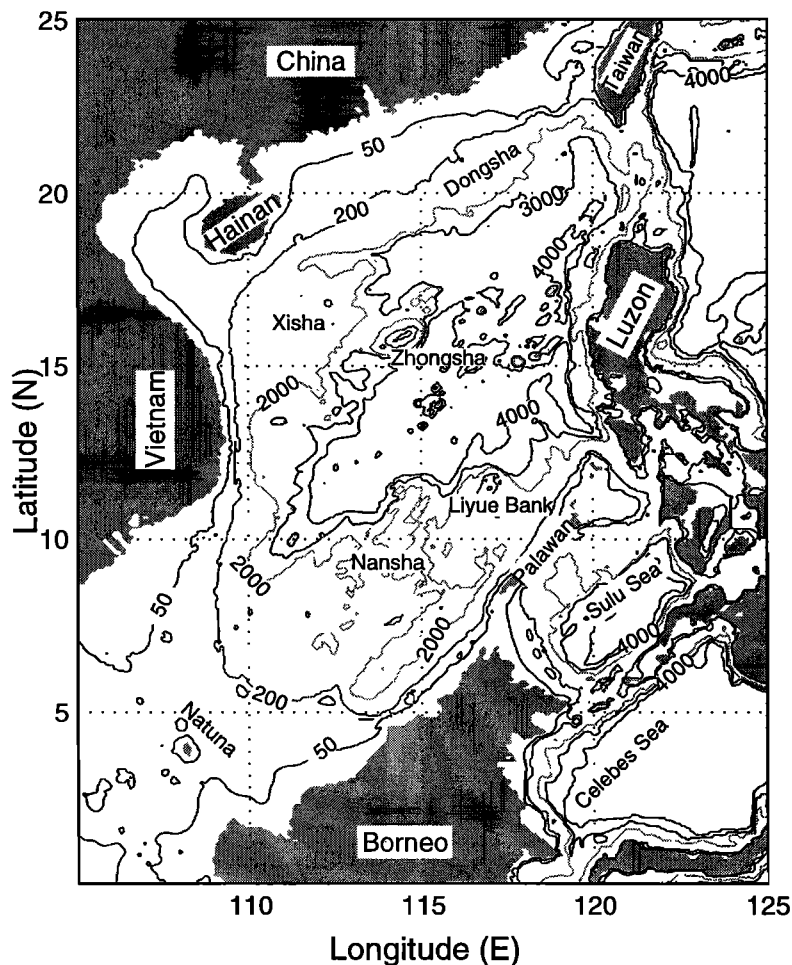
Figure 1. Geography and isobaths showing the bottom topography of the South China Sea.

cember 29, 1993, to January 5, 1994, from the analysis of TOPEX/ POSEIDON data [*Soong et al.* 1995]. *Chu et al.* [1997a] and *Chu and Chang* [1997] identified the existence of a central SCS surface warm-core eddy in mid-May from a historical data set: the U.S. Navy's Master Observational Oceanographic Data Set (MOODS). From the composite analysis on the U.S. National Centers for Environmental Prediction (NCEP) monthly sea surface temperature (SST) fields (1982-1994), *Chu et al.* [1997b] found that during the spring-to-summer monsoon transition (March-May) a warm anomaly (greater than 1.8°C) is formed in the central SCS at 112°-119°30'E, 15°-19°30'N.

All of these analyses were based on the sea surface data. What is the subsurface thermal structure and circulation pattern of the SCS eddies? The Naval Oceanographic Office conducted an intensive airborne expendable bathythermograph (AXBT) survey between May 14-25, 1995, over the majority of the SCS down to about 300 m depth. Figure 3 shows the daily AXBT deployment. This data set provides something close to a "snapshot" of the temperature in the upper ocean in the SCS during the transition time before the onset of the monsoon. Since only temperature-measuring AXBTs were used, no salinity measurements were made

at the same time. We will invert three-dimensional eddy features from analysis of this temperature data set using climatological salinity data [*Levitus*, 1984] in lieu of in situ salinity data.

The outline of this paper is as follows. A description of the AXBT measurement and establishment of gridded data is given in section 2. A depiction of the β spiral method with two necessary conditions is given in section 3. The synoptic three-dimensional thermal structure and inverted velocity field is discussed in section 4. In section 5 we present our conclusions.

2. AXBT Measurements

Most of the 376 AXBTs were deployed at six intervals over a 12 day period from May 14-25, 1995 (Figure 3). The majority of the AXBTs were nominally capable of reaching a depth of 360-400 m. The ensemble of temperature profiles (Figure 4a) and the mean profile with an envelope of a standard deviation (Figure 4b) show the existence of a mixed layer with depths ranging from 20 to 60 m and a thermocline with a vertical temperature gradient of 6°-7°C per 100 m below the mixed layer.
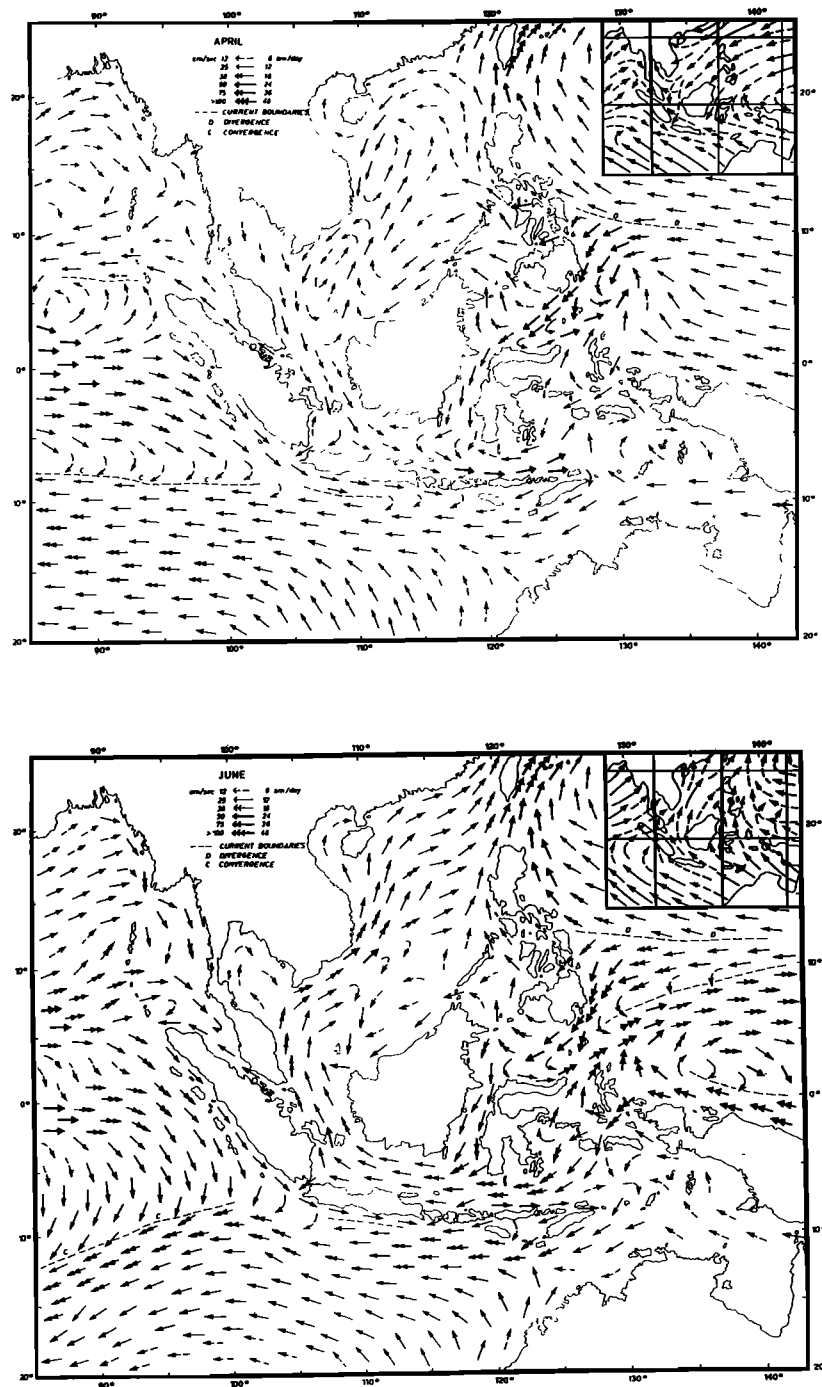
The AXBT observations were mapped to a regular

Figure 2. A drastic change of the surface circulation from (a) April to (b) June [after *Wyrtki*, 1961].

grid at 12 levels (Table 1) using a two-scale optimal interpolation (OI) scheme [*Gandin*, 1965; *Lozano et al.*, 1996]. The large-scale OI was used to estimate the background mean with a decorrelation scale of 450 km. The mesoscale OI was used to map the observational anomaly from the background mean field into a regular grid with a spatial decorrelation scale of 75 km and a temporal decorrelation scale of 10 days. The spatial and temporal decorrelation scales associated to the mean field was estimated from the covariance matrix obtained from MOODS for the SCS [see *Chu et al.*, 1997c]. The large-scale mean was computed using the temperature and salinity profiles. The large-scale pattern for the surface (not shown) resembles the pattern previously estimated by *Chu et al.* [1997c]. The decorrelation length scale for the fluctuations from the mean was estimated from the AXBT data. The results shown below are relatively insensitive to the length scale in the range of 60-90 km. The decorrelation timescale was selected to ensure synopticity. The SST horizontal scales seem somewhat larger than temperatures in the seasonal thermocline. In this study, we choose horizon-
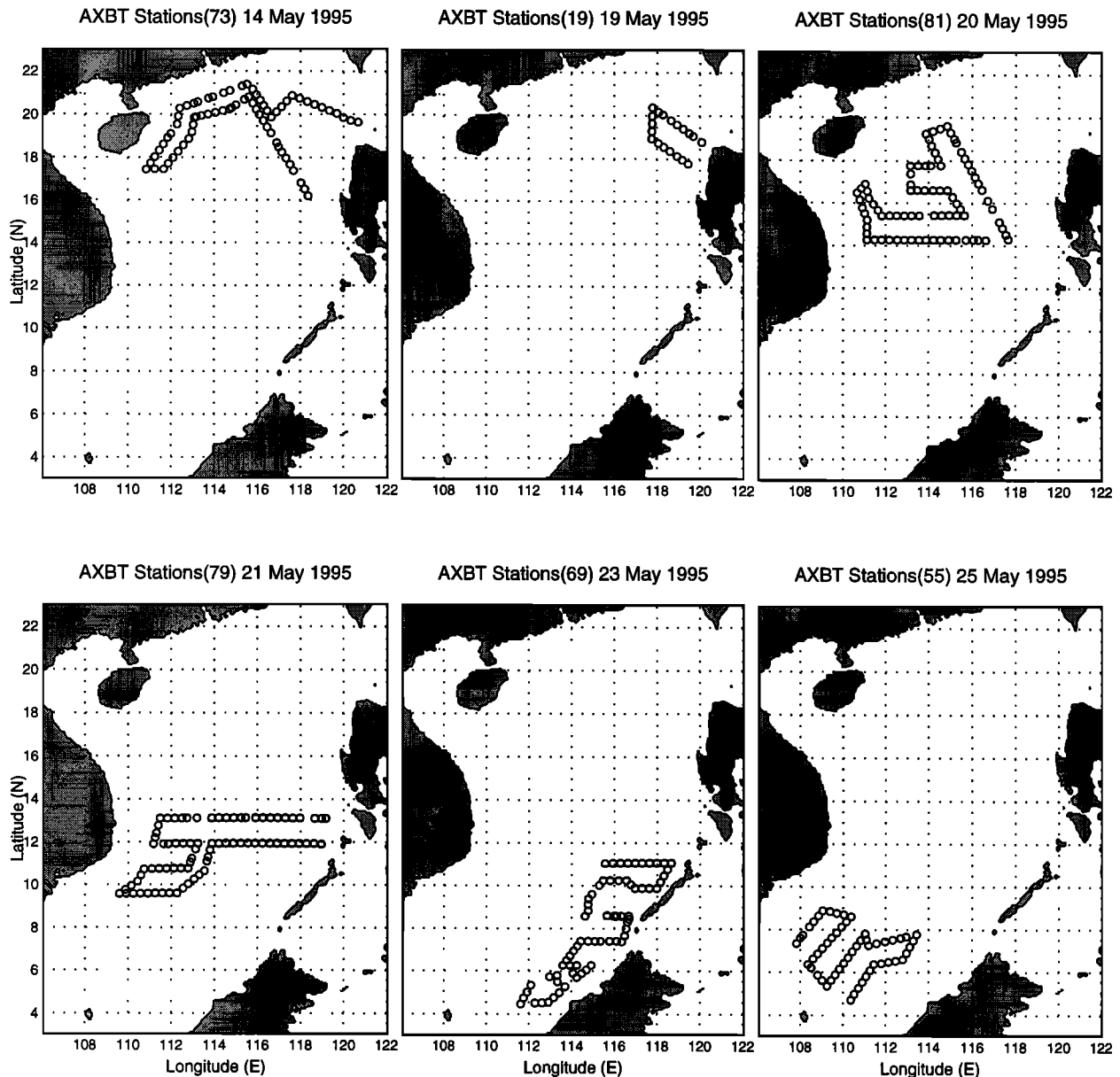
Figure 3. Deployment pattern of AXBT survey during May 14-25, 1995.

tal scales to be uniform in the vertical for convenience and for lack of sufficient data to discriminate these differences properly.

3. β Spiral Method

3.1. Geostrophic Velocity Inverted from Density Field

Often the thermal wind relation is employed to calculate geostrophic velocity from hydrographic data

$$u = u_0 + \frac{g}{f\rho_0} \int_{z_0}^{z} \frac{\partial \hat{\rho}}{\partial y} dz' \tag{1}$$

$$v = v_0 - \frac{g}{f\rho_0} \int_{z_0}^{z} \frac{\partial \hat{\rho}}{\partial x} dz' \tag{2}$$

where (u, v) and (u_0, v_0) are the geostrophic velocity at

any depth z and at a reference depth z_0, $\hat{\rho}$ is the in situ water density, ρ_0 is the characteristic value of the density, $f = 2\Omega \sin \lambda$, is the Coriolis parameter, where Ω is the Earth's rotation rate and λ is the latitude. The hydrographic data determine the geostrophic vertical shear. The reference velocity (u_0, v_0) remains undetermined. On the basis of the geostrophic and hydrostatic balances and mass conservation equations, several inverse techniques have been developed to compute the geostrophic velocity at the reference level (u_0, v_0). These include the β spiral method [Stommel and Schott, 1977; Schott and Stommel, 1978], the box inverse method [Wunsch, 1978], and the Bernoulli method [Killworth, 1986]. Wunsch [1994] proposed a generalized β spiral and geostrophic balance inverse method based on a nonlinear optimization on Needler's P equation [Needler, 1967]. (See the review paper on the β spiral method by Olbers et al. [1985].) Davis [1978] pointed out that the
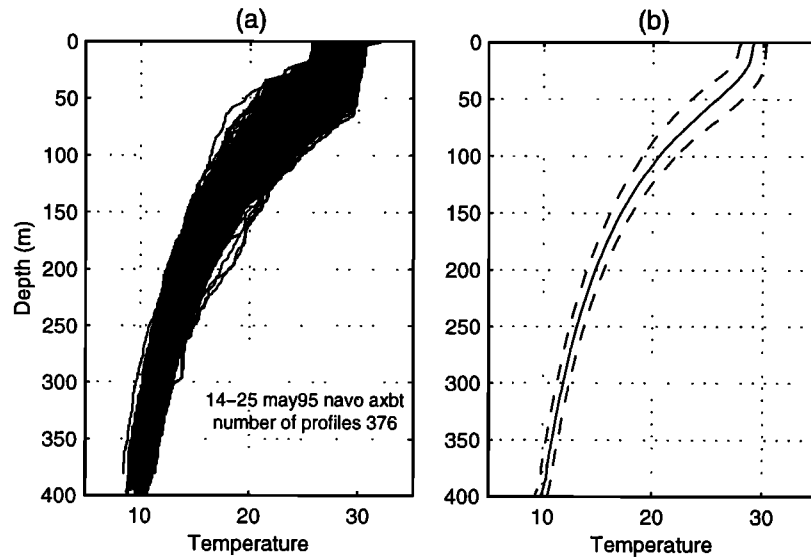
Figure 4. Temperature profiles of AXBT survey during May 14-25, 1995. (a) Ensemble of profiles and (b) the mean profile with an envelope of a standard deviation. Both show the existence of a mixed layer with depths ranging from 20 to 60 m and a thermocline with a vertical temperature gradient of $6°$-$7°$C/100 m below the mixed layer.

β spiral method and the box inverse method, no matter how different in appearance, are based on the same dynamical assumptions, and the existence of the β spiral thus becomes a required condition for these inverse methods.

Recently, nongeostrophic inverse methods were also developed. *Bogden et al.* [1993] estimated the time-averaged velocity field in the North Atlantic from observations of density, wind stress, and bottom topography based on the assumption of minimum mixing of potential density at middepth. *Tziperman et al.* [1992] applied the adjoint method to investigate the steady state oceanic general circulation using a realistic numerical oceanic general circulation model and hydrographic data.

As pointed out by *Wunsch and Grant* [1982], in determining large-scale circulation from hydrographic data, we can be reasonably confident of the assumptions of geostrophic balance, mass conservation, and no major cross-isopycnal mixing (except for water masses in contact with the atmosphere). Under these conditions, the density of each fluid element would be conserved, which mathematically is given by

$$\mathbf{V} \bullet \nabla\rho = 0 \tag{3}$$

where ρ is the potential density and $\mathbf{V} = (u, v, w)$ is the geostrophic velocity. The conservation of potential vorticity equation [*Pedlosky*, 1986] can be obtained by differentiating (3) with respect to z, using geostrophic and hydrostatic balances, and including the latitudinal variation of the Coriolis parameter to give

$$\mathbf{V} \bullet \nabla q = 0 \tag{4}$$

where $q = f\partial\rho/\partial z$. Use of $f\partial\rho/\partial z$ may induce a small but systematic error into estimation of potential vorticity [*G. T. Needler*, unpublished manuscript, 1986]. Equations (3) and (4) imply that the velocity $\mathbf{V}$ is parallel to $\nabla q \times \nabla\rho$.

3.2. Necessary Conditions for Validity of the β Spiral Method

Stommel and Schott [1977] pointed out that the three-dimensional velocity field cannot be determined from the density field alone when the q and ρ surfaces coincide. The first necessary condition for the validity of this inverse method thus is

1. Necessary Condition 1: The ρ surface is not parallel to the q surface, which mathematically requires

$$\nabla\rho \times \nabla q \neq 0 \tag{5}$$

Stommel and Schott [1977] further pointed out that the three-dimensional velocity field cannot be determined from the ρ field alone if the horizontal velocity does not rotate with depth (β spiral). The existence of the β spiral is the second necessary condition.

2. Necessary Condition 2: The velocity (u, v) should execute a β spiral, which mathematically requires that for at least two depths, $z = z_k$, and $z = z_m$, with horizontal velocities $[u^{(k)}, v^{(k)}]$ and $[u^{(m)}, v^{(m)}]$,

$$\begin{vmatrix} u^{(k)} & v^{(k)} \\ u^{(m)} & v^{(m)} \end{vmatrix} \neq 0 \tag{6}$$

If we cannot find levels z_k and z_m such that (6) is satisfied, the inverse method will fail to get velocity in that water column.

Table 1. Vertical Levels of the Interpolated Temperature Field

Level	Depth (m)
1	0
2	10
3	20
4	30
5	50
6	75
7	100
8	125
9	150
10	200
11	250
12	300

3.3. Implementation of the Necessary Conditions

Consider the unit vector $\mathbf{P}$ [Chu, 1995] defined by

$$\mathbf{P} = \frac{\nabla\rho \times \nabla q}{|\nabla\rho \times \nabla q|} \qquad (7)$$

The existence of this unit vector implies the satisfaction of necessary condition 1.

The velocity, $\mathbf{V} = (u, v, w)$, parallels the unit vector $\mathbf{P}$,

$$\mathbf{V} = r(x, y, z)\mathbf{P} \qquad (8)$$

where r is the proportionality. Applying the thermal wind relation at two different depths z_k and z_m, as shown in Figure 5a, a set of algebraic equations for determining the parameter r are obtained

$$r^{(k)}P_x^{(k)} - r^{(m)}P_x^{(m)} = \Delta u_{km}$$

$$r^{(k)}P_y^{(k)} - r^{(m)}P_y^{(m)} = \Delta v_{km} \qquad (9)$$

which are two linear algebraic equations for $r^{(k)}$ and $r^{(m)}$ [$r^{(i)} = r(x, y, z_i)$]. Here

$$(\Delta u_{km}, \Delta v_{km}) = \frac{g}{f\rho_0} \int_{z_m}^{z_k} (\frac{\partial\widehat{\rho}}{\partial y}, -\frac{\partial\widehat{\rho}}{\partial x})dz' \qquad (10)$$

The determinant of (9)

$$\begin{vmatrix} P_x^{(k)} & P_x^{(m)} \\ P_y^{(k)} & P_y^{(m)} \end{vmatrix} = \sin(\alpha_{km}) \qquad (11)$$

is the sine of the vertical turning angle between $\mathbf{P}_h^{(k)}$ and $\mathbf{P}_h^{(m)}$ (Figure 5b); that is, α_{km} is the β spiral turning angle between the two levels z_k and z_m. The algebraic equations in (9) have definite solutions for $r^{(k)}$

$$r^{(k)} = \frac{\begin{vmatrix} \Delta u_{km} & P_x^{(m)} \\ \Delta v_{km} & P_y^{(m)} \end{vmatrix}}{\sin(\alpha_{km})} \qquad (12)$$

if

$$\alpha_{km} \neq 0 \qquad (13)$$

As soon as $r^{(k)}$ ($k = 1, 2, ...$) is obtained, the absolute velocity field can be calculated by (8). Before using the inverse method, we should check for the two necessary conditions (5) and (6) or, equivalently, (7) and (13).

For water columns satisfying the two necessary conditions, we may use (13) to compute $r^{(k)}$ for the level z_k. There are N-1 sets ($m = 1, 2, k$-1, k+1, ... N) of equations (9) for calculating $r^{(k)}$. Here N is the total
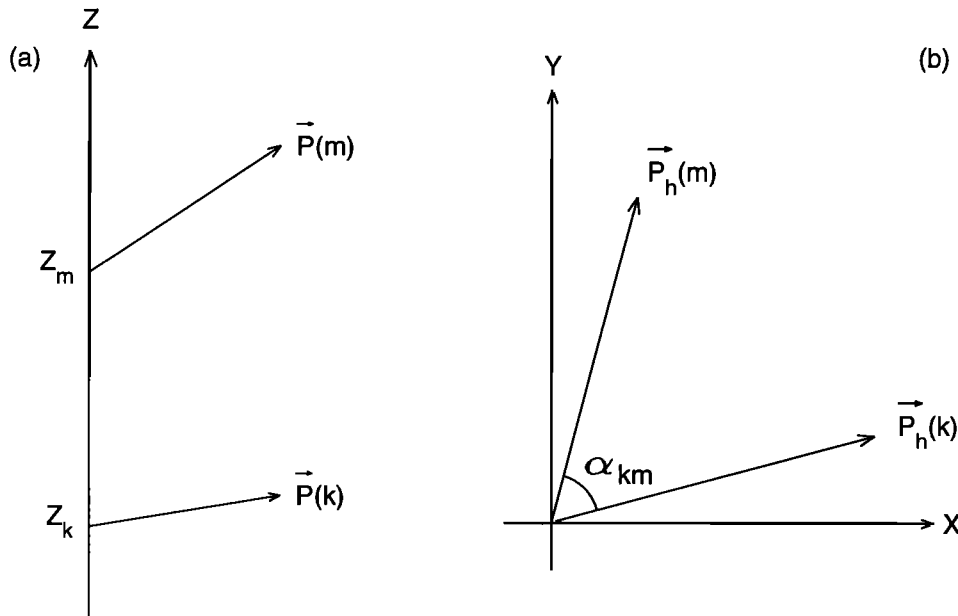

Figure 5. Vertical turning of the $\mathbf{P}$ vector. (a) $\mathbf{P}$ vector at two different levels and (b) turning angle between two levels.
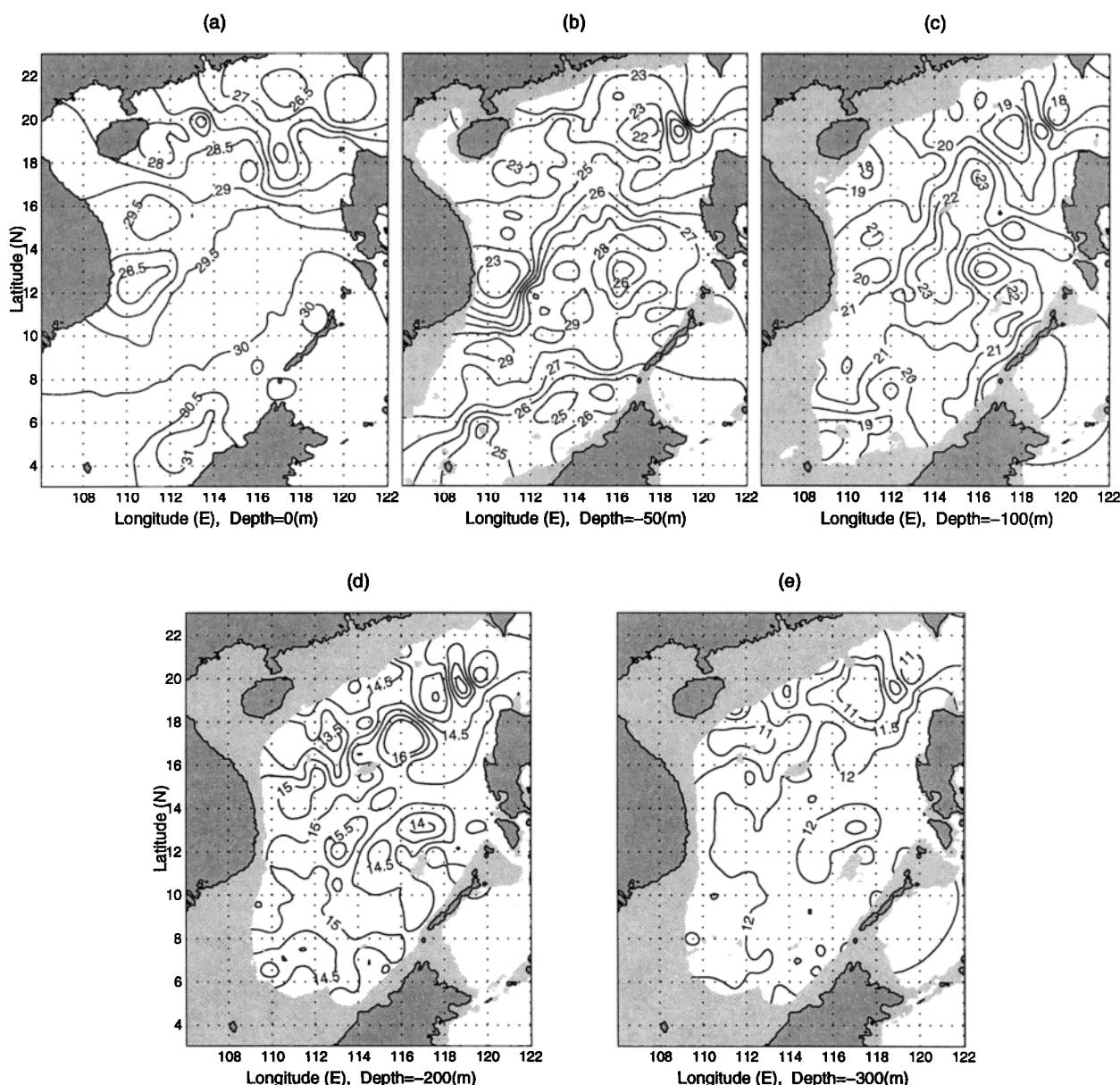
Figure 6. Horizontal temperature fields at different depths: (a) 0 m, (b) 50 m, (c) 100 m, (d) 200 m, and (e) 300 m. The central SCS warm pool was surrounded by Dongsha (DS), Hainan (HN), South-Vietnam (SV), and Liyue (LY) cool pools and Xisha (XS) warm pool.

number of vertical levels of the water column. All the N-1 sets of equations are compatible under the thermal wind constraint and should provide the same solution. However, because of errors in measurements (instrumentation errors) and computations (truncation errors), the parameters $r^{(k)}$ may vary with m. A least squares error algorithm (appendix A) is used to minimize the error. For further details and validation of the algorithm presented here see *Chu et al.* [1998]. Interested readers can obtain the software by contacting Mr. Chenwu Fan at fan@nps.navy.mil or visiting our Web site at http://web.nps.navy.mil/~chu.

4. Results

4.1. Thermal Field

4.1.1. Horizontal structures. Figures 6a-6e are horizontal depictions of temperature at 0, 50, 100, 200, and 300 m depths, respectively. The contour interval is 0.5°C. In them, we see that warmer water is situated at the central SCS with surrounding cooler water. At the 50 m depth, the 28°C isotherm separates the warm central SCS water from the surrounding cooler water. The maximum temperature reaches 29°C. This

Table 2. Locations, Typical Temperatures, and Tangential Velocity of the SCS Warm-Core and Cool-Core Eddies Appearing During May 14-25, 1995

Depth (m)	Central SCS (W)	Xisha (W)	Dongsha (C)	Hainan (C)	South Vietnam (C)	Liyue (C)
0	112°-117°E	110°-112°E	116°-118°20'E	110°-112°E	108°-112°E	115°-118°E
	12°-18°N	14°-16°N	18°-20°20'N	18°-20°N	10°-14°N	12°-14°N
	29.5°-30°C	29.5°C	27°C	28°C	28.5°C	29.5°-30°C
	40 cm/s	20 cm/s	40 cm/s	10 cm/s	20 cm/s	30 cm/s
50	112°-117°E	110°-112°E	116°-118°20'E	110°-112°E	108°-112°E	115°-118°E
	12°-18°N	14°-16°N	18°-20°20'N	16°-18°N	10°-14°N	12°-14°N
	29°C	24°C	22°C	23°C	23°C	26°C
	30 cm/s	10 cm/s	25 cm/s	8 cm/s	10 cm/s	30 cm/s
100	112°-117°E	110°-112°E	116°-118°20'E	109°-111°30'E	110°-112°E	115°-118°E
	12°-18°N	14°-15°N	18°-20°20'N	16°40'-19°N	12°-14°N	12°-14°N
	23°C	21°C	18°C	18°C	20°C	19°C
	25 cm/s	8 cm/s	20 cm/s	5 cm/s	10 cm/s	20 cm/s
200	112°-117°E	110°-112°E	116°-118°20'E	109°-113°E		114°-117°E
	12°-18°N	14°-15°N	18°-20°20'N	16°-18°N		11°-14°N
	16°C	15°C	13°C	13.5°C		14°C
	10 cm/s	4 cm/s	10 cm/s	4 cm/s		9 cm/s
300	115°-117°E	···	116°-118°20'E	110°-113°E		114°-116°E
	16°-18°N	···	18°-20°20'N	16°-18°N		10°-14°N
	12°C	···	11°C	11°C	···	11.5°C
	2 cm/s	···	3 cm/s	1 cm/s		3 cm/s

central SCS warm pool extended to the 300 m depth and was surrounded by Dongsha (DS), Hainan (HN), South-Vietnam (SV), and Liyue (LY) cool pools and Xisha (XS) warm pool. The location and thermal features of these warm and cool pools are listed in Table 2.

4.1.2. Vertical structures. Four zonal cross sections (19°N, 17°N, 13°N, and 7°N) of temperature show the vertical structure of the mixed layer and the thermocline as well as the warm and cool pools (Figure 7). The mixed layer was not evident at the 19°N cross section but develops as latitude decreases. For the 17°N and 7°N cross sections, the mixed layer shallows toward the east. In the 13°N cross section, the mixed layer deepens at 114°E. The trough and ridge of the isotherms may be considered as centers of warm and cool pools.

The 19°N cross section clearly shows the existence of DS cool pool near 117°E from the uplifting (ridge) of isotherms. The ridge is located at 117°E at the surface, eastward shifted with depth, and kept at 117°E below the 100 m depth. The longitudinal span of DS cool pool is around 2°.

The two cross sections at 17°N and 13°N show the occurrence of a central SCS warm pool from the downward bending (trough) of isotherms: 116°E at 17°N and 114°E at 13°N. The longitudinal span of central SCS warm pool is around 4° for both latitudes. The warm water is nearly isolated from the surrounding cooler water. This may suggest that local forcing might be important for the central SCS warm pool formation.

The 7°N cross section shows the eastward uplift of the thermocline depth from 50 m at 110°E to 25 m at 115°E. A surface warm pool with SST higher than

30°C was found between 112°-115°E, and a midlevel (100 m) cool pool was detected between 110°-112°E. In the eastern part (113°-115°E), an isolated warm pool appeared below the 175 m depth.

Three latitudinal cross sections (111°E, 114°E, and 117°E) of temperature also show the vertical structure of the mixed layer and the thermocline as well as the warm and cool pools (Figure 8). The mixed layer had a shallow-deep-shallow pattern in the latitudinal direction. Taking the 114°E cross section as an example, the mixed layer had a shallow depth (about 10 m) near 5°N. Its depth increased with latitude to about 60 m at 13°30'N and decreased with latitude to almost zero (no mixed layer) near 20°N.

The "trough" and "ridge" of the isotherms may be considered as centers of warm and cool pools. The three cross sections indicated the occurrence of central SCS warm eddy evident from the downward bending (trough) of isotherms: 9°N at the 111°E, 13°N at 114°E, and 15°N and 17°N at 117°E.

4.2. The SCS Circulation

4.2.1. T-S and T-S̄ relations. The β spiral method was used to determine the velocity field from hydrographic data. Since there were no salinity (S) observations in SCS during May 14-25, 1995, May climatological salinity [Levitus, 1984] was interpolated to the AXBT stations and those salinity values (S̄) were used for the P vector computation. To validate this technique, we plotted two T-S diagrams: One diagram (Figure 9a) is the plot of 3478 T, S profiles from MOODS in May between 1933-1986 and the other diagram (Fig-
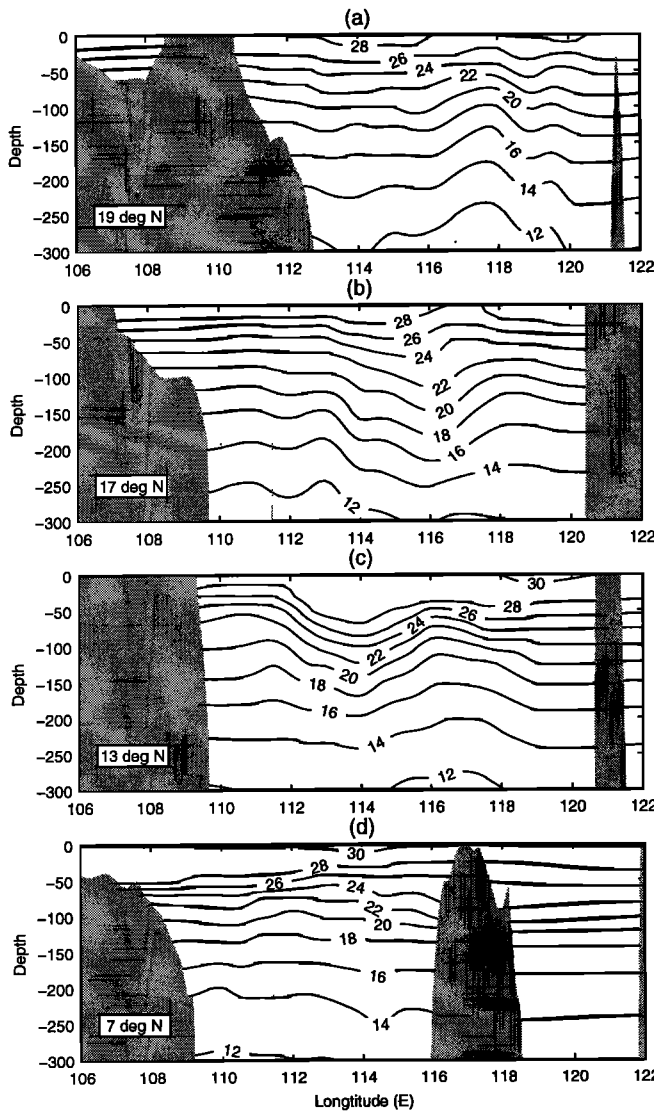
Figure 7. Temperature distribution at several zonal cross sections: (a) 19°N, (b) 17°N, (c) 13°N, and (d) 7°N.

rounded by several cyclonic and anticyclonic eddies. Generally, the anticyclonic (cyclonic) eddies are associated with the warm (cool) pools. The kinetic features of these eddies are listed in Table 2. Furthermore, the magnitude of inverted velocities decreases with depth and is quite small at 300 m. This implies that a diagnostic method with a level of no motion at or below about a 300 m depth could have been used to give results close to the β spiral method.

The observed three-dimensional temperature and inverted velocity fields indicate the existence of a central SCS warm-core anticyclonic eddy with surrounding DS, HN, SV, and LY cool-core cyclonic eddies and XS warm-core anticyclonic eddy (Figure 12).

4.2.3. Zonal cross sections of v component. Four zonal cross sections (19°N, 17°N, 13°N, and 7°N) of v velocity show the vertical eddy structure (Figure 13). The positive values indicate northward velocity, and the negative values refer to the southward velocity. Alternate positive and negative areas indicate the occurrence of cyclonic and anticyclonic eddies. At each zonal cross section, a neighboring eastern negative/western positive pattern refers to an anticyclonic eddy, and, a neighboring western negative/eastern positive pattern refers to a cyclonic eddy.

The 19°N cross section clearly shows the existence of the DS cyclonic eddy near 117°E. The diameter of the DS eddy is around 300 km. The depth of the eddy is around 200 m. This eddy reveals an asymmetric fea-
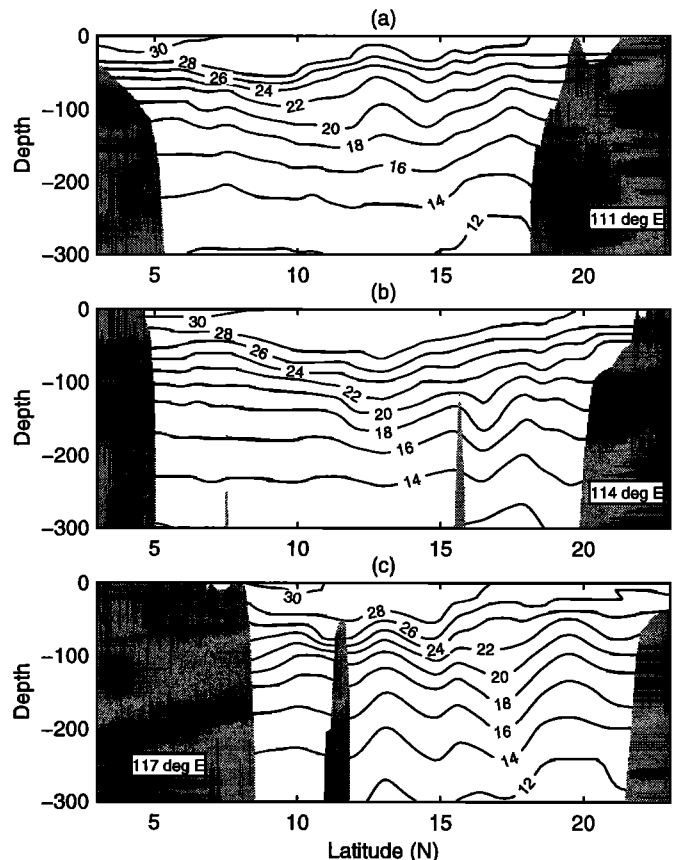
ure 9b) is the plot of 376 T (AXBT) and $\overline{S}$ profiles. The spatial and temporal distributions of the MOODS data are illustrated in Figures 10a and 10b. Comparison between the two diagrams shows that the T-S characteristics remain stable. However, we should be aware of the shortcomings in using the climatological salinity values ($\overline{S}$). If the temperature field is relatively homogeneous in space, the density gradient depends mostly on the salinity gradient. Under that circumstance, the use of the climatological salinity values may bring large errors in inverting the velocity field.

4.2.2. Horizontal velocity fields. The available historical data [*Wyrtki*, 1961] show two totally different circulation patterns for the months preceding and following the AXBT survey in the central SCS: a cyclonic gyre in April (Figure 2a) and an anticyclonic gyre in June (Figure 2b). We may treat the May circulation as the transition between the two patterns.

Our inverted velocity data set (Figure 11) indicates the existence of a central SCS anticyclonic gyre sur-

Figure 8. Temperature distribution at several latitudinal cross sections: (a) 111°E, (b) 114°E, and (c) 117°E.
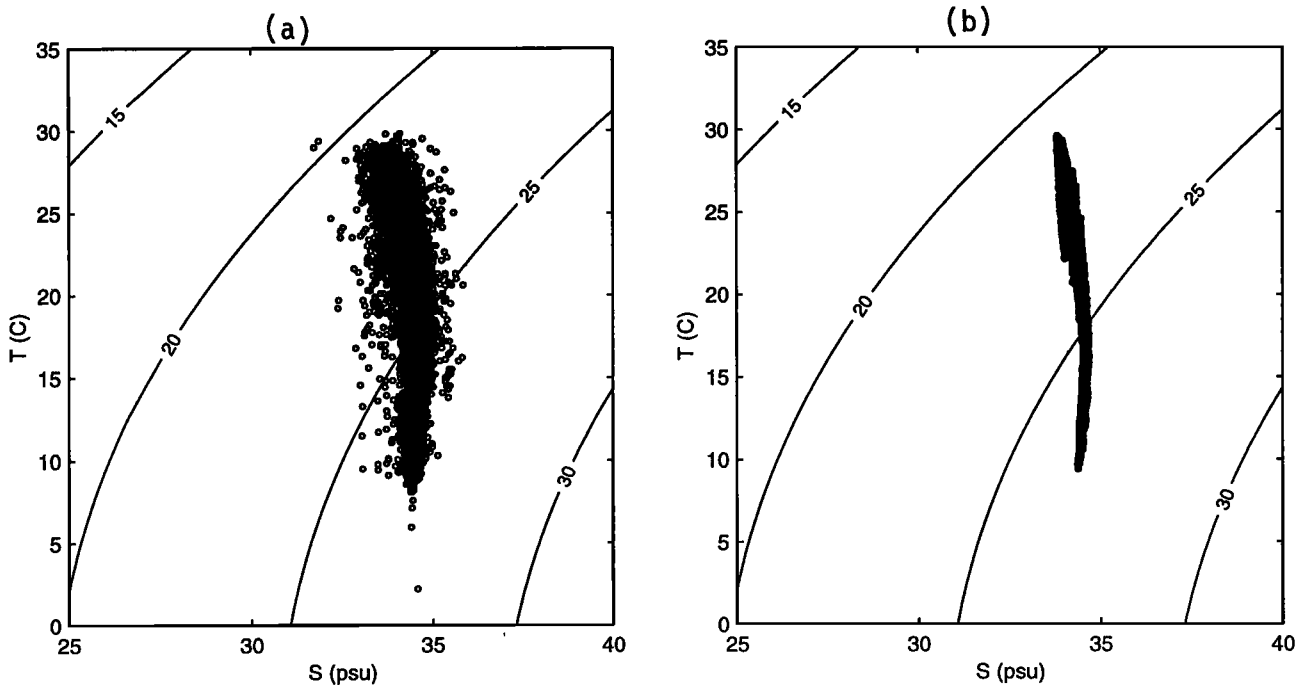
Figure 9. T-S diagrams for (a) the Navy's MOODS data set in May between 1933-1986 and (b) the AXBT temperature and May climatological salinity.

ture. The northward velocity with a maximum speed of 40 cm/s in the eastern part is much stronger than the southward velocity with a maximum speed of 10 cm/s in the western part.

The 17°N cross section clearly shows the existence of the central SCS anticyclonic eddy centered at 116°E. The zonal span of the central SCS eddy is around 500 km. The depth of the eddy is around 300 m. The maximum tangential velocity is around 20 cm/s. This

eddy is quite symmetric with a maximum southward velocity in the eastern part similar to the northward velocity in the western part.

The 13°N cross section clearly shows the existence of a double-eddy structure. Between 112°E and 116°E there was a strong anticyclonic eddy (the central SCS eddy) with a maximum tangential speed of 30 cm/s (appearing in the upper 50 m) and centered at 114°E. The zonal span of this eddy is around 500 km. This anti-
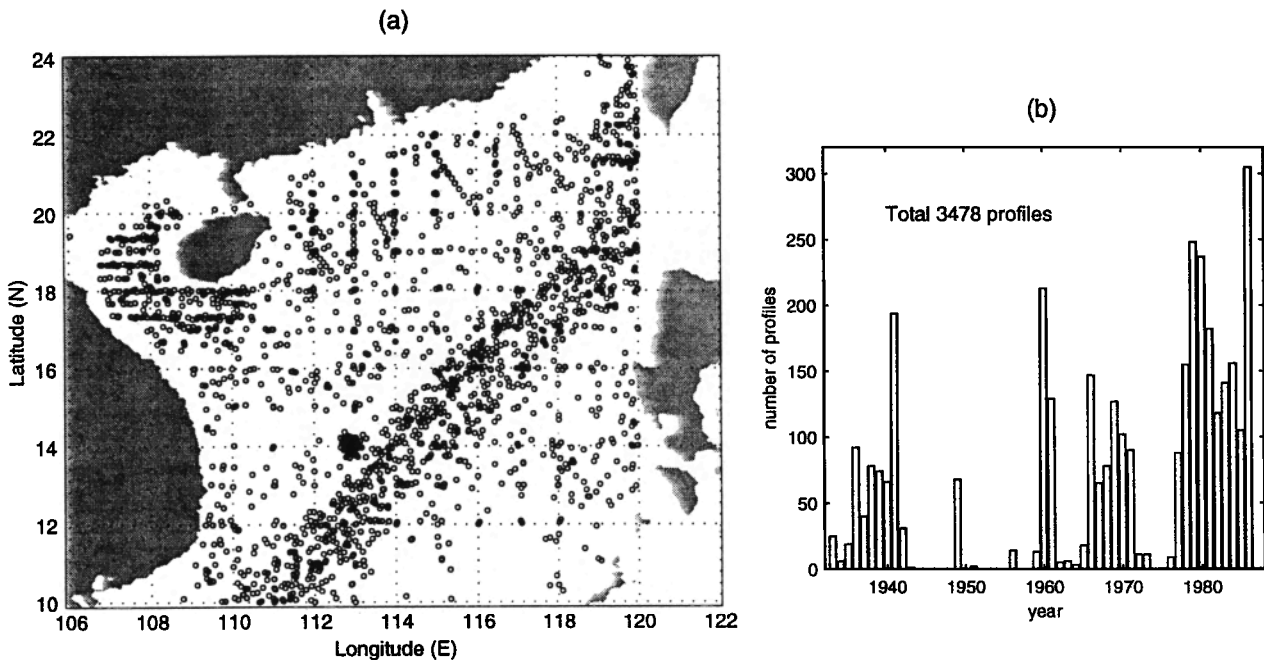

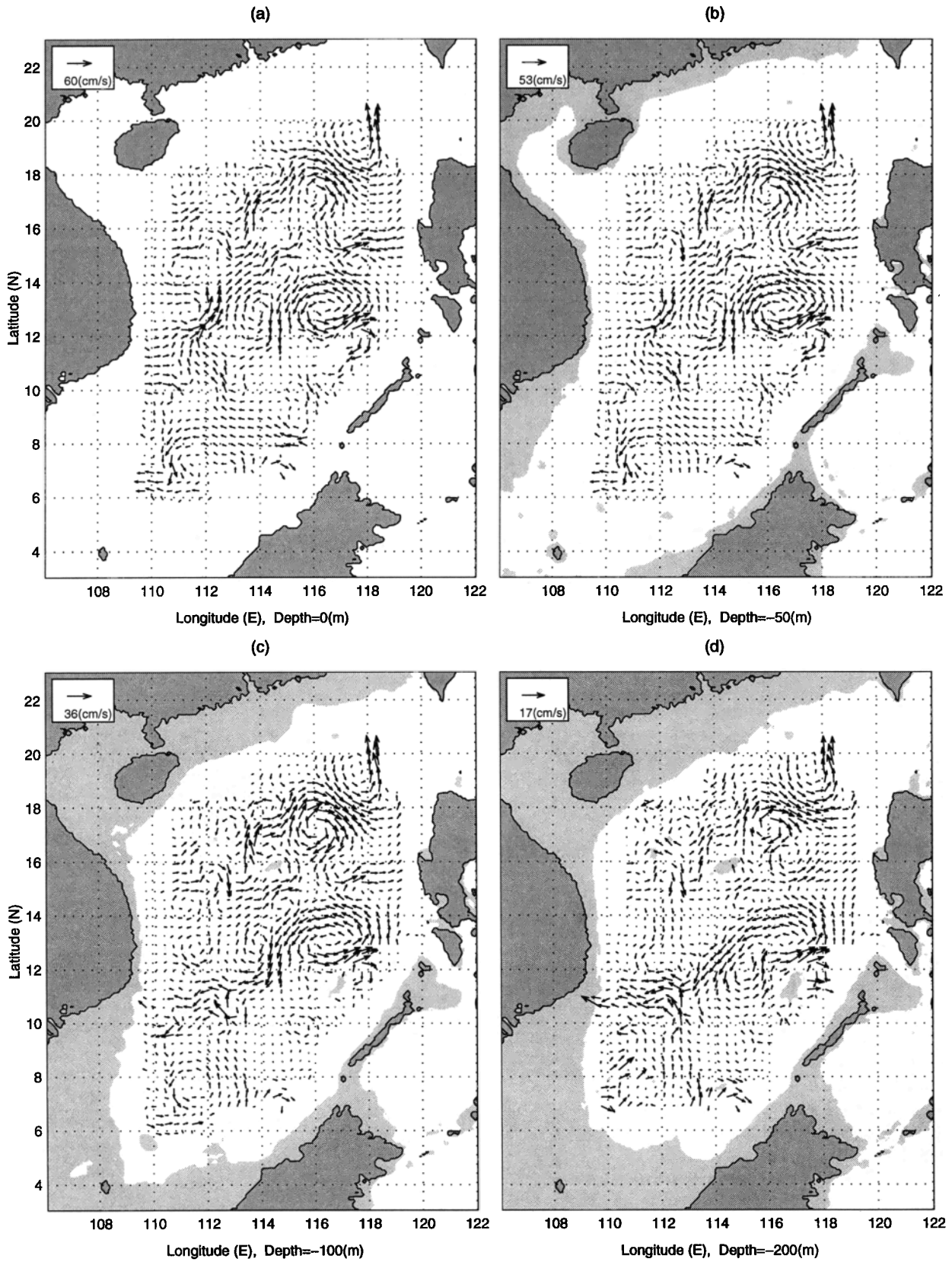**Figure 10.** MOODS data distribution: (a) spatial and (b) temporal.

Figure 11. Absolute velocity at different depths: (a) 0 m, (b) 50 m, (c) 100 m, (d) 200 m, and (e) 300 m. The central SCS anticyclonic eddy was surrounded by DS, HN, SV, and LY cyclonic eddies and XS anticyclonic eddy.
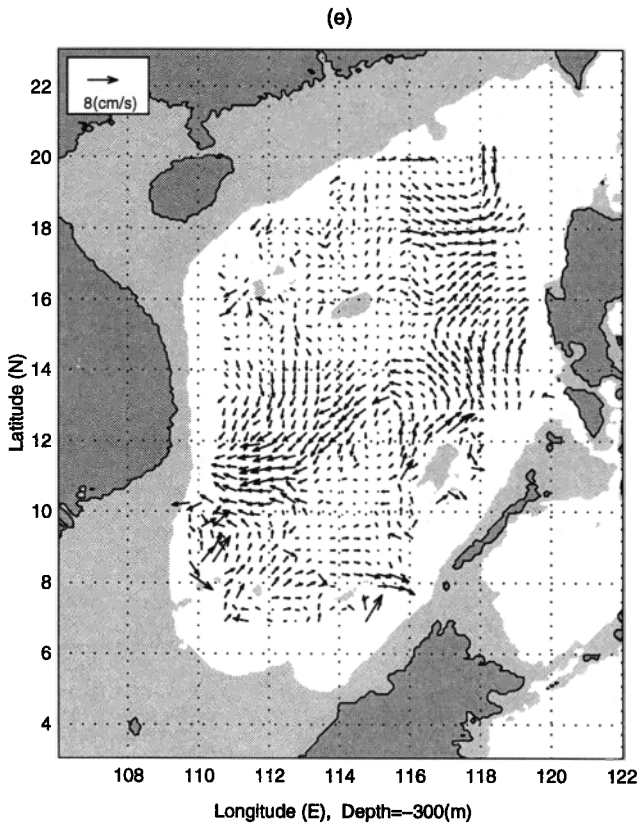
(e)

Figure 11. (continued)

cyclonic eddy is associated with the central SCS warm pool. The depth of the eddy is around 250 m. To the east of the anticyclonic eddy, a cyclonic eddy appeared between 114°E to 119°E centered at 116°20'E. This cyclonic eddy is associated with the LY cool pool, and therefore called the LY cool-core (cyclonic) eddy. The central SCS warm-core eddy and LY cool-core eddy shared the same southward branch. Furthermore, the northward flow at the eastern part of the LY cool-core eddy (maximum tangential speed around 10 cm/s) is much weaker than the southward flow in the western part.

The 7°N cross section shows the occurrence of a cyclonic eddy (110°-114°E). This cyclonic eddy is quite asymmetric. The southward flow (maximum tangential speed around 20 cm/s) in the western part is stronger than the northward flow (maximum tangential speed around 10 cm/s) in the eastern part. The depth of the eddy is around 150 m. To the east of the anticyclonic eddy, a cyclonic eddy appeared between 114°E to 119°E centered at 116°20'E.

4.2.4. Latitudinal cross sections of u component. Three latitudinal cross sections (111°E, 114°E, and 117°E) of u velocity also show the vertical eddy structure (Figure 14). The positive values indicate eastward velocity, and the negative values refer to westward velocity. Alternate positive and negative areas indicate the occurrence of cyclonic and anticyclonic eddies. At each latitudinal cross section, a neighboring southern negative/northern positive pattern refers to an anticyclonic eddy. However, a neighboring northern

negative/southern positive pattern refers to a cyclonic eddy.

The area with a southern negative/northern positive u pattern (anticyclonic eddy) coincides with the area of the downward bending isotherms (warm pool). At the 111°E cross section, the central SCS warm-core eddy is recognized by an isotherm trough located at 9°N (Figure 12), and an anticyclonic eddy is identified by the southern negative/northern positive u pattern centered at 9°N (Figure 13). At the 114°E cross section, the central SCS warm-core eddy is recognized by an isotherm trough located at 13°N (Figure 12), and an anticyclonic eddy is identified by the southern negative/northern positive u pattern centered at 13°N (Figure 13).

4.3. Comparison With Previous Work

This snapshot of multi-eddy structure agrees quite well with previous studies of individual SCS eddies appearing in mid-May. For example, the central SCS warm-core eddy was previously reported by the South China Sea Institute of Oceanology [SCSIO, 1985] and identified as a recurring phenomenon by analyzing historical data such as MOODS [Chu et al., 1997a] and NCEP monthly SST [Chu et al., 1997b]. The surrounding smaller cool-core and warm-core eddies were identified separately by different authors. The DS cool-core eddy was identified by He et al. [1996] and the SV cool-core eddy was reported by Dale [1956] and Uda and Nakao [1972]. Our contribution here is to present a synoptic multi-eddy structure in mid-May, the monsoon transition period.

4.4. Mechanisms

In searching for mechanisms for the formation of this recurring seasonal signal, a central SCS warm anomaly, Chu et al. [1997b] found a high correlation between surface wind stress curl and SST anomaly from correlation analysis of the European Center for Medium-range Weather Forecast (ECMWF) analyzed wind stress data and the NCEP SST data. The high correlation leads to a hypothesis for the wind-driven central SCS warm pool during the spring-to-summer monsoon transition. The bowl-type bottom topography shown in Figure 1 provides a favorable condition for the central SCS warm pool formation in the spring-to-summer monsoon transition. In spring, a surface anticyclone usually appears over the central SCS [Cheang, 1987]. Ekman downwelling will occur in the central part of the "bowl," and mass balance will cause upwelling near the boundary of the "bowl." The downwelling prevents the deep cold water from advecting upward, while the upwelling along the boundary helps the deep cold water advect upward. This makes the central part of the "bowl" warm and the side part of the "bowl" cool and leads to the generation of the central SCS warm pool surrounded by several cool pools. Furthermore, other mechanisms such as remote forcing and topographic influence could be significant.

5. Conclusions

1. Objective analysis of the AXBT data allowed us to identify the occurrence of a warm pool in the central
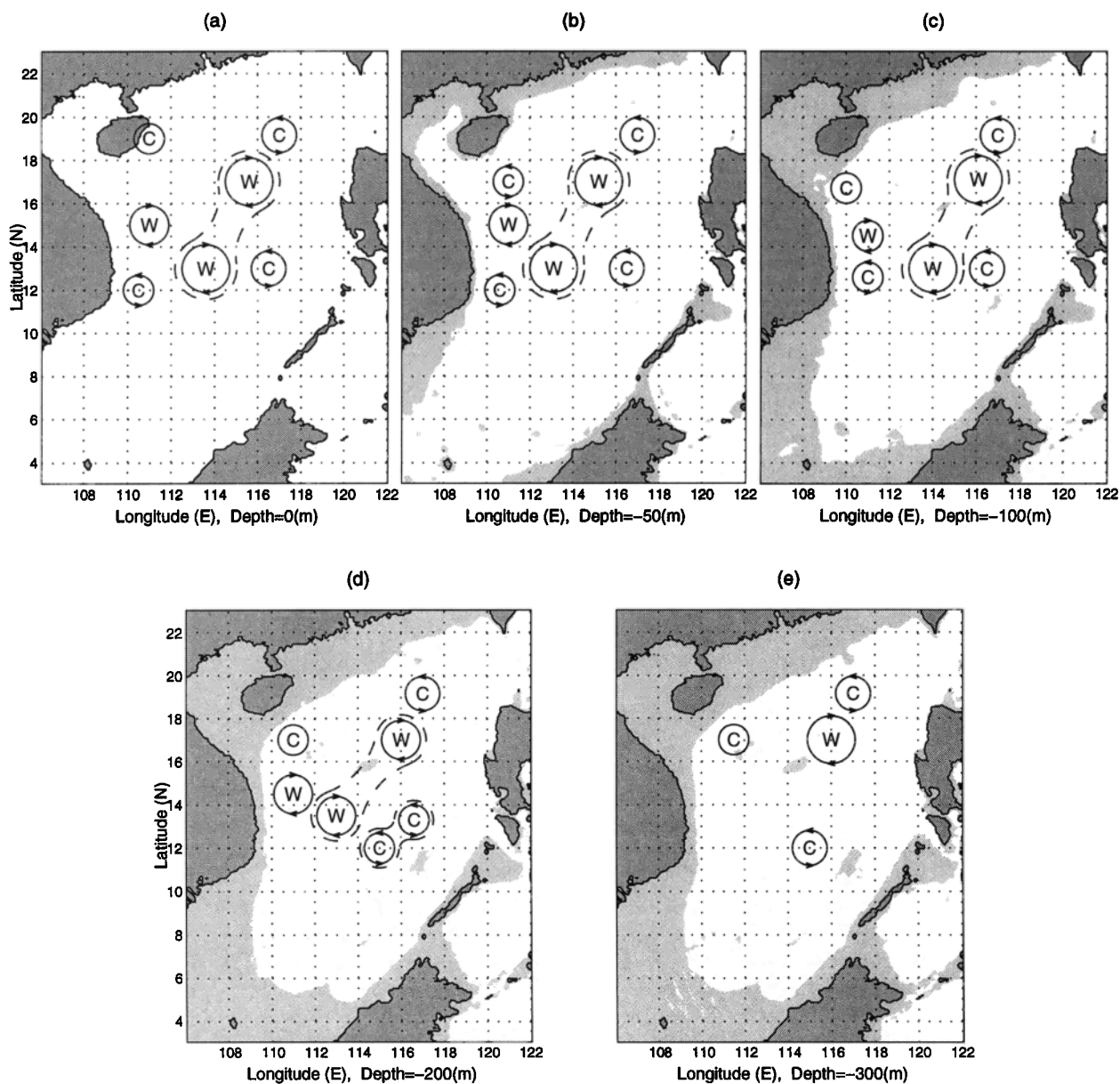
Figure 12. Illustration of South China Sea warm-core and cool-core eddies in May 1995.

SCS during May 14-25, 1995. The maximum SST of this warm pool reached 29.5°C and higher. This warm pool extended to the SCS southern boundary at the surface and became more isolated in the central SCS below the surface. Its size was near 200,000 km² at 50 m depth and decreased with depth. The double anti-cyclonic eddies derived from the inverse method were colocated with the central SCS warm pool and had a maximum tangential velocity around 40 cm/s.

2. The central SCS warm eddy was surrounded by several cool-core and warm-core eddies with a radius of around 100 km and maximum tangential velocities ranging from 10 cm/s to 40 cm/s. The cool-core eddies were cyclonic and warm-core eddies were anticyclonic. The inverted velocity field shows the existence of XS warm-core anticyclonic eddy with a maximum tangential velocity of 20 cm/s, strongest between the surface

and 100 m depth, DS cool-core cyclonic eddy with a maximum tangential velocity of 40 cm/s, strongest between the surface and 200 m depth, SV cool-core cyclonic eddy between surface and 100 m depth with a maximum tangential velocity of 20 cm/s at surface and decreasing with depth, LY cool-core cyclonic eddy with a maximum tangential velocity of 30 cm/s, strongest between the surface and 50 m depth, and HN cool-core cyclonic eddy with a maximum tangential velocity of 10 cm/s, the weakest of the cool-core eddies.

3. The central SCS warm-core eddy identified in the May 1995 AXBT measurements is a recurring phenomenon. The results obtained in this study agree well with the historical data analyses such as the MOODS and NCEP monthly sea surface data set.

4. The wind-driven mechanism for the formation of a central SCS warm-core eddy with surrounding cool-core
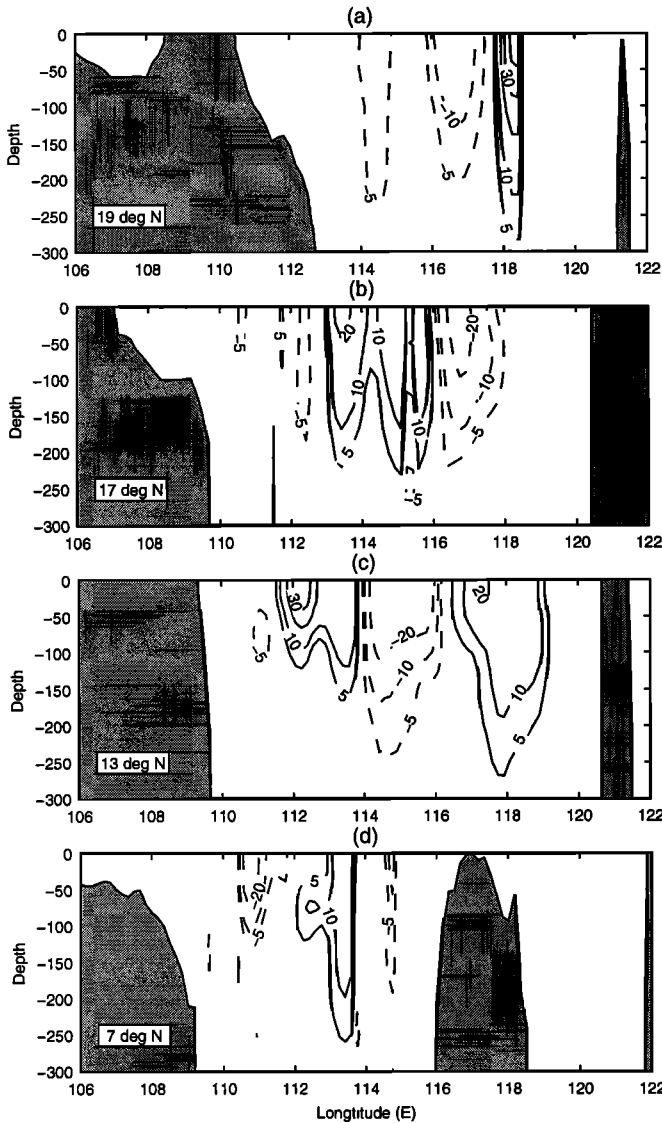
Figure 13. Distribution of velocity v component at several zonal cross sections: (a) 19°N, (b) 17°N, (c) 13°N, and (d) 7°N.

eddies during the spring-to-summer transition was confirmed by a numerical study. A manuscript on this modeling study was submitted to the Journal of Oceanography for publication.

Appendix: Optimization Scheme

If the absolute velocity $(u^{(k)}, v^{(k)})$ is known, we may use the thermal wind relation (10) to obtain the absolute velocity at any level m,

$$u^{(m)} = u^{(k)} + \Delta u_{mk}, \quad v^{(m)} = v^{(k)} + \Delta v_{mk}$$

$$w^{(m)} = -\frac{u^{(m)}\partial\rho^{(m)}/\partial x + v^{(m)}\partial\rho^{(m)}/\partial y}{\partial\rho^{(m)}/\partial z}$$

The computed $\left[u^{(m)}, v^{(m)}, w^{(m)}\right]$ may not be in the same direction as the **P** vector $\left[P_x^{(m)}, P_y^{(m)}, P_z^{(m)}\right]$ at the

level m. If we assume that the **P** vector exists at the level m and that the velocity vector parallels the vector $\mathbf{P}^{(m)}$, an error can be easily defined by (Figure 15)

$$E_m = |V^{(m)}\mathbf{P}^{(m)} - \mathbf{V}^{(m)}| = 2\sin\left[\tfrac{1}{2}(\widehat{\mathbf{P}^{(m)}, \mathbf{V}^{(m)}})\right] V^{(m)}$$
$$\simeq V^{(m)}\sin(\widehat{\mathbf{P}^{(m)}, \mathbf{V}^{(m)}})$$

where $V^{(m)} = |\mathbf{V}^{(m)}|$ and $(\widehat{\mathbf{P}^{(m)}, \mathbf{V}^{(m)}})$ is the angle between $\mathbf{P}^{(m)}$ and $\mathbf{V}^{(m)}$. The total error of the water column velocity caused by the uncertainty of $(u^{(k)}, v^{(k)})$ is

$$E = \sqrt{\sum_m (h_m E_m)^2}$$

where h_m is the thickness of the mth layer (see Table 1).

We determine the velocity $(u^{(k)}, v^{(k)})$ such that the total error E becomes minimum; that is,

$$\frac{\partial E}{\partial u^{(k)}} = 0, \quad \frac{\partial E}{\partial v^{(k)}} = 0$$

which leads to a 2×2 algebraic equations for determining $(u^{(k)}, v^{(k)})$,

$$A_{11}u^{(k)} + A_{12}v^{(k)} = F_1$$
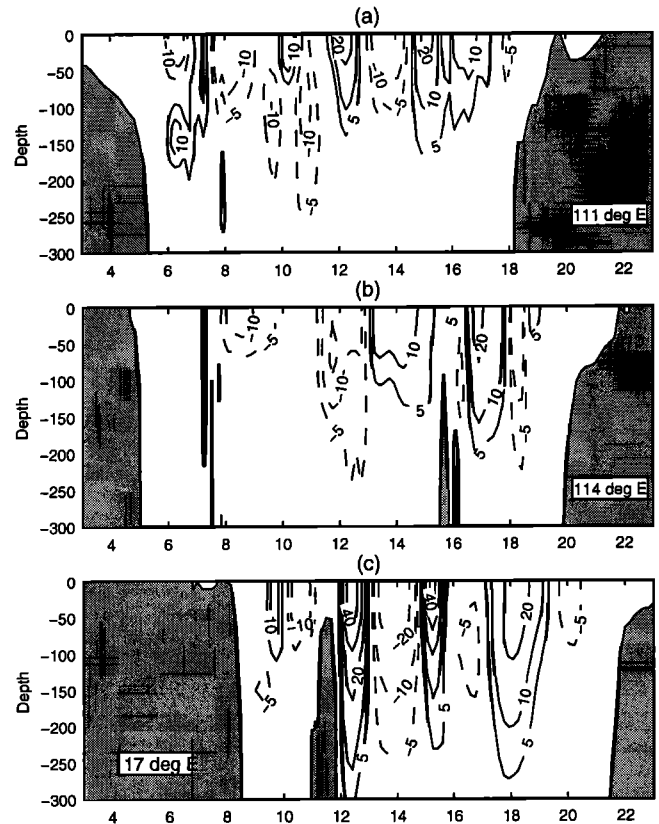$$A_{21}u^{(k)} + A_{22}v^{(k)} = F_2$$

Figure 14. Distribution of velocity u component at several latitudinal cross sections: (a) 111°E, (b) 114°E, and (c) 117°E.
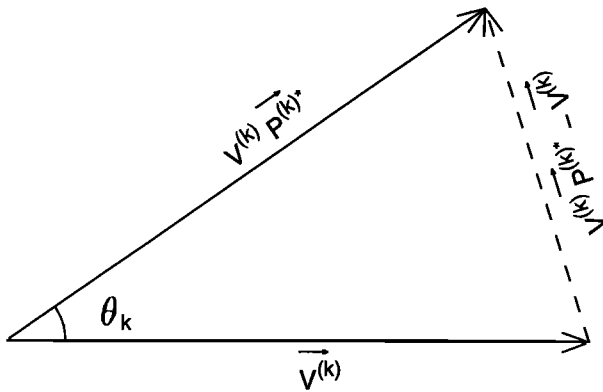
Figure 15. Error caused by the uncertainty of the velocity at the level k.

where

$$A_{11} = \sum_m a_{11}^{(m)}, \qquad A_{12} = \sum_m a_{12}^{(m)}$$
$$A_{12} = A_{21}, \qquad A_{22} = \sum_m a_{22}^{(m)}$$
$$F_1 = -\sum_m (a_{11}^{(m)} \Delta u_{mk} + a_{12}^{(m)} \Delta v_{mk})$$
$$F_2 = -\sum_m (a_{21}^{(m)} \Delta u_{mk} + a_{22}^{(m)} \Delta v_{mk})$$

and

$$a_{11}^{(m)} \equiv (P_y^{(m)})^2 f^{(m)}, \qquad a_{12}^{(m)} \equiv -P_x^{(m)} P_y^{(m)} f^{(m)}$$
$$a_{22}^{(m)} \equiv (P_x^{(m)})^2 f^{(m)}$$
$$f^{(m)} \equiv \left[1 + \left(\frac{\partial \rho^{(m)}/\partial x}{\partial \rho^{(m)}/\partial z}\right)^2 + \left(\frac{\partial \rho^{(m)}/\partial y}{\partial \rho^{(m)}/\partial z}\right)^2\right] h_m^2$$

The absolute velocity at the level $z = z_k$ can be computed by

$$u^{(k)} = \frac{F_1 A_{22} - F_2 A_{12}}{A_{11} A_{22} - A_{12} A_{21}}, \qquad v^{(k)} = \frac{F_2 A_{11} - F_1 A_{21}}{A_{11} A_{22} - A_{12} A_{21}}$$

Thus the second necessary condition becomes that if

$$A_{11} A_{22} - A_{12} A_{21} = 0 \qquad (14)$$

the inverse method fails.

References

Bogden, P.S., R.E. Davis, and R. Salmon, The North Atlantic circulation: combining simplified dynamics with hydrographic data. *J. Mar. Res.*, 51, 1-52, 1993.

Cheang, B.K., Some aspects of winter monsoon and its characteristics in Malaysia, *Res. Publ. No.2*, Maylaysian Meteorological Service, Kuala Lumpur, 1980.

Chu, P.C., P vector method for determining absolute velocity from hydrographic data, *Mar. Technol. Soc. J.*, 29(3), 3-14, 1995.

Chu, P.C., and C.P. Chang, South China Sea warm pool in boreal spring, *Adv. Atmos. Sci.*, 14, 195-206, 1997.

Chu, P.C., H. C. Tseng, C.P. Chang, and J.M. Chen,

South China Sea warm pool detected in spring from the Navy's Master Oceanographic Observational Data Set (MOODS), *J. Geophys. Res.*, 102, 15,761-15,771, 1997a.

Chu, P.C., S.H. Lu, and Y.C. Chen, Temporal and spatial variabilities of the South China Sea surface temperature anomaly, *J. Geophys. Res.*, 102, 20,937-20,955, 1997b.

Chu, P.C., S.K. Wells, S.D. Haeger, C. Szczechowski, and M. Carron, Temporal and spatial scales of the Yellow Sea thermal variability, *J. Geophys. Res.*, 102, 5,655-5,667, 1997c.

Chu, P.C., C.W. Fan, and W.J. Cai, Evaluation of P vector method using modular ocean model (MOM), *J. Oceanogr.*, 54, 185-198, 1998.

Dale, W.L., Winds and drift currents in the South China Sea, *Malayan J. Trop. Geogr.*, 8, 1-31, 1956.

Davis, R., On estimating velocity from hydrographic data, *J. Geophys. Res.*, 83, 5507-5509, 1978.

Gandin, L.S., Objective Analysis of Meteorological Fields. Israel Program for Scientific Translation, Jerusalem, 242 pp., 1965.

He, Y., C. Guan, and H. Gao, Water temperature and circulation structure in the upper ocean of the northern South China Sea (in Chinese with English abstract), *Oceanography in China*, Vol. 6, pp. 60-69, Ocean Press, Beijing, 1996.

Huang, Q.Z., W.Z. Wang, Y.S. Li, and C.W. Li, Current characteristics of the South China Sea, *Oceanology of China Seas*, edited by D. Zhou, Y.B. Liang, and C.K. Tseng, Kluwer Acad., Norwell, Mass., 1994.

Killworth, P., A Bernoulli inverse method for determining the ocean circulation, *J. Phys. Oceanogr.*, 16, 2031-2051, 1986.

Levitus, S., Climatological atlas of the world ocean, *NOAA Prof. Pap.* 13, Nat. Oceanic Atmos. Admin., Silver Spring, Md., 1984.

Lozano, C.J., A.R. Robinson, H.G. Arango, A. Gangopadhyay, Q. Sloan, P.J. Haley, L. Anderson, and W. Leslie, An interdisciplinary ocean prediction system: Assimilation strategies and structure data model, *Modern Approaches to Data Assimilation in Ocean Modeling*, edited by P. Malanotte-Rizzoli, pp. 413-452, Elsevier, New York, 1996.

Needler, G.T., A model for the thermohaline circulation in an ocean of finite depth, *J. Mar. Res.*, 25, 329-342, 1967.

Nitani, H., Oceanographic conditions in the sea east of Philippines and Luzon Strait in summer of 1965 and 1966, *The Kuroshio-A Symposium on Japan Current*, edited by J.D. Marr, pp. 213-232, East-West Press, Honolulu, Hawaii, 1970.

Olbers, D.J., M.Wenzel, and J. Willbrand, The inference of North Atlantic circulation patterns from climatological hydrographic data, *Rev. Geophys.*, 23, 313-356, 1985.

Pedlosky, J., Thermocline theories, *General Circulation of the Ocean*, edited by H.G.I. Abardanel and W.R. Young, pp.55-101, Springer-Verlag, New York, 1986.

Schott, F., and H. Stommel, Beta spirals and absolute velocities in different oceans, *Deep Sea Res.*, 25, 961-1010, 1978.

Soong, Y.S., J.H. Hu, C.R. Ho, and P.P. Niiler, Cold-core eddy detected in South China Sea, *Eos Trans. AGU*, 76, 345-347, 1995.

South China Sea Institute of Oceanology, Integrated Investigation Report on Sea Area of the South China Sea (in Chinese), Vol. 2, pp. 183-231, Science Press, Beijing, 1985.

Stommel, H., and F. Schott, The beta spiral and the determination of the absolute velocity field from hydrographic station data, *Deep Sea Res.*, 24, 325-329, 1977.

Tziperman, E., W.C. Thacker, R.B. Long, and S.-H. Hwang, Oceanic data analysis using a general circulation model, 1, Simulations, *J. Phys. Oceanogr.*, 22, 1434-1457, 1992.

Uda, M. and T. Nakao, Water masses and currents in the South China Sea and their seasonal changes, Paper presented at *the 3rd Cooperative Study of the Kuroshio and Adjacent Regions (CSK) Symposium*, UNESCO, Bangkok, Thailand, 1972.

Wunsch, C., The general circulation of the North Atlantic west of 50°W determined from inverse method, *Rev. Geophys.*, 16, 583-620, 1978.

Wunsch, C., Dynamically consistent hydrography and absolute velocity in the eastern North Atlantic Ocean. *J. Geophys. Res.*, 99, 14,071-14,090, 1994.

Wunsch, C., and B. Grant, Towards the general circulation of the North Atlantic Ocean, *Prog. Oceanogr.*, 11, 1-59, 1982.

Wyrtki, K., Scientific results of marine investigations of the South China Sea and Gulf of Thailand 1959-1961, *Naga Rep., 2*, pp. 164-169, Scripps Institution of Oceanography, University of California, San Diego, 1961.

P.C. Chu, and C. Fan, Department of Oceanography, Naval Postgraduate School, Monterey, CA 93943. (e-mail: chu@nps.navy.mil; fan@nps.navy.mil)

J.L. Kirling, N311, Naval Oceanographic Office, Stennis Space Center, MS 39529. (e-mail: kerlingj@navo.navy.mil)

C.J. Lozano, Department of Earth and Planetary Sciences, Harvard University, Cambridge, MA 02138. (e-mail: lozano@alboran.harvard.edu)